

https://doi.org/10.1070/QEL17269

Lasing efficiency of krypton ions in the (8–14)-nm band upon pulsed laser excitation

A.N. Nechay, S.A. Garakhin, A.Ya. Lopatin, V.N. Polkovnikov, D.G. Reunov, N.N. Salashchenko, M.N. Toropov, N.I. Chkhalo, N.N. Tsybin

Abstract. **The emission spectra of krypton plasma in the range of 8–14 nm upon excitation of a pulsed gas jet by 1.06-μm Nd:YAG laser radiation with a pulse energy of 0.85 J, pulse duration of 5.2 ns, and repetition rate of 10 Hz are investigated. The krypton emission spectrum is a wide (8–14 nm) band, peaking at 10.3 nm, which is formed by a series of much narrower lines. The observed lines are identified, and the fraction of laser pulse energy converted into the (8–14)-nm emission band and emitted into half-space (2π sr) is determined. The maximum conversion efficiency is found to be 21%. The expected throughputs of lithographic systems with sources based on Sn, Xe, and Kr ions for different wavelengths, corresponding to the emission peaks of ions of these materials, are compared.**

Keywords: *laser spark, krypton plasma, extreme UV radiation, pulsed gas target, conversion efficiency, lithography.*

1. Introduction

Progress in the field of microelectronics is closely related to the reduction of chip characteristic sizes. For example, 10-nm resolution was achieved in classical lithography [1], and studies aimed at further improving the resolution (in particular, applying short-wavelength lithography) are actively under way. The extreme UV (EUV) lithography using the wavelength λ = 13.5 nm provides a resolution within 7–10 nm under laboratory conditions [2, 3]. However, as was discussed in [4], further attempts to increase resolution meet very serious problems in increasing the numerical aperture of the EUV objective even to NA = 0.5. In this context, the decrease in the wavelength of next-generation projection lithography is a very urgent task.

Previously the prospects of implementing a lithographic process at λ = 6.7 nm were considered in [5, 6], and the specific features of using radiation with this wavelength in lithography were analysed in detail in [7]. It was shown that, with allowance for the reflectance of multilayer La/B4C mirrors [8], the X-ray source efficiency, and the photoresist sensitivity [9–11], the throughput of a lithographic process at λ = 6.7 nm is an order of magnitude lower than that at λ = 13.5 nm.

A.N. Nechay, S.A. Garakhin, A.Ya. Lopatin, V.N. Polkovnikov, D.G. Reunov, N.N. Salashchenko, M.N. Toropov, N.I. Chkhalo, N.N. Tsybin Institute for Physics of Microstructures, Russian Academy of Sciences, ul. Akademicheskaya 7, 603087 Afonino, Kstovskii raion, Nizhny Novgorod region, Russia; e-mail: dima@ipm.sci-nnov.ru

Received 6 February 2020
Kvantovaya Elektronika **50** (4) 408–413 (2020)
Translated by Yu.P. Sin'kov

Based on the experimental data on the efficiency of Xe-based laser-plasma source [12–14] and the reflectances of multilayer mirrors Mo/Be [15] and Mo/Sr, Ru/Sr [16], it was shown that a lithographic process with a throughput comparable with that obtained at λ = 13.5 nm can be implemented at λ = 11.2 and 10.8 nm. It was noted that, to confirm these suggestions, one must measure the exact values of the laser energy conversion efficiency into EUV radiation and determine the real reflectances of Be- and Sr-based multilayer mirrors.

An analysis of the emission spectra of xenon ions under pulsed laser excitation and measurements of the conversion efficiency using a calibrated X-ray power meter were performed in [17, 18]. A pulsed gas-jet target was used [19]. The laser conversion efficiency into soft X-rays (SXR) was about 1.6% in the lithographer transmission band peaking at λ = 10.8 nm and about 1% at λ = 10.2 nm. Later on, these values were confirmed in [20, 21]. Thus, the xenon source conversion efficiency turned out to be almost several times lower than that of the tin source [22]. Another drawback of the source based on xenon is the high cost of this gas.

The interest in the SXR source based on inert gas ions has significantly increased in view of the development of maskless X-ray lithography, where throughput is not a critically important parameter. The ranges of application of maskless lithography are mainly related to the research in the field of science and technology and to the small-scale production; important factors in these applications are high resolution, availability of equipment, and its low operation cost [23–26]. Advantages of inert gases for lithography of this type are the absence of contaminations of optics with tin and a shorter working wavelength, due to which the spatial resolution can be significantly increased in comparison with the lithography using a wavelength of 13.5 nm.

In this study we investigated the emission from ions of krypton, which is known to be a heavy inert many-electron gas and have a complex of favourable properties to be used as an efficient target in laser-plasma SXR sources. One can state that the emission properties of krypton in the SXR range have been scarcely studied. In particular, there are no data in the literature on the laser energy conversion efficiency into SXR. For example, a wide emission band at 8–14 nm and a high-intensity band peaking near 10.3 nm were shown to exist for krypton [19]. The emission of highly ionised krypton upon laser excitation was also investigated in [27]. Thus, the main purpose of this study was to measure the conversion efficiency, analyse the influence of different parameters (such as the gas pressure at the capillary inlet and the distance from the laser spark to the capillary edge) on the conversion effi-

ciency, and search for the experimental conditions providing maximum conversion efficiency of laser radiation into X rays.

2. Experimental

Emission spectra were studied on an experimental setup whose schematic is shown in Fig. 1 [28]. It consists of a solid-state pulsed laser, a gas jet former (a radiation source), and an RSM-500 spectrometer with a spherical grating and power meter (calibrated in the SXR range) [29]. The laser beam is introduced into a vacuum chamber and focused on pulsed gas jet, which is formed by a pulsed valve. A breakdown with the formation of high-temperature plasma occurs in the region of the laser beam focus. The laser spark radiation is recorded simultaneously by a spectrometer and a power meter.

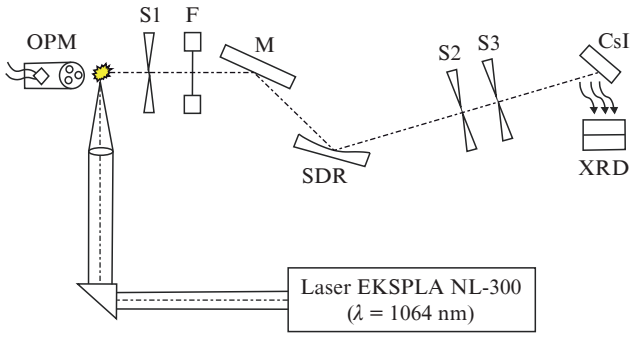

Figure 1. Setup for studying the emission characteristics of laser-excited krypton:
(OPM) calibrated power meter; (S1–S3) slits; (F) short-wavelength filter; (M) mirror; (SDR) spherical diffraction grating; (XRD) X-ray detector VEU-7 (chevron type microchannel converter).

A laser spark was excited using a NL300 EKSPLA pulsed laser with a radiation wavelength of 1.06 μm, laser pulse energy of 0.85 J, pulse duration of 5 ns, and pulse repetition rate of 10 Hz. The laser beam was directed into the vacuum chamber using a prism, and then focused by a lens on the axis of a pulsed gas target. The average laser power was measured by an IMO-2N power meter. Because of the loss in the optical system, the laser pulse energy in the spark region amounted to 0.56 J.

Krypton was fed using a high-speed pulsed valve (synchronised with the laser); it effused through a capillary 0.4 mm in diameter. The concentration of krypton atoms in the laser-spark formation region was about 10^{18} cm^{-3} [18, 30]. The maximum krypton pressure reached 5 bar; it was limited by the characteristics of the pumping system in use. The gas-jet source was described in more detail in [31]. The design of the setup made it possible to orient the gas jet perpendicular to the spectrometer optical axis, due to which the self-absorption of the radiation generated in the plasma affected the measurement results to a lesser extent. The measurements were carried out in the spectral range of 4–20 nm, and the spectral resolution was 0.04 nm. The radiation at the monochromator output arrived at a CsI photocathode to generate an electron current, which was detected using a chevron assembly of two microchannel converters (VEU-7). The spectrometer was evacuated by two cryosorption pumps and, additionally, a turbomolecular pump with a pumping rate of 100 L s^{-1}. The experiments were performed at a pressure of 2×10^{-5} Torr in the detector chamber and 1×10^{-3} Torr in the radiation source chamber. To estimate the possible influence of plasma absorption lines on the measurement results, we performed additional measurements of krypton emission spectra in the geometry with spectrometer optical axis coinciding with the gas nozzle axis. A Czerny–Turner spectrometer [32] was applied.

The conversion efficiency of laser radiation into SXR was measured using a calibrated power meter (Fig. 1). The X-ray power was determined by applying a set of free-standing thin-film filters and a silicon photodiode, which directly recorded SXR. The photodiode sensitivity was calibrated in the entire spectral range on the BESSY-II synchrotron source [33]. The spectral characteristics of the filters were measured with a reflectometer [34] at characteristic emission lines. There was a possibility of introducing one or two free-standing Mo/$ZrSi_2$ filters; they were mounted on a special holder and could be replaced automatically during an experiment. The operation principle and design features of the power meter were described in more detail in [35]. To obtain the maximum conversion efficiency, we first found the optimal time of valve open state τ_{op} (it turned out to be 300 μs) and the optimal delay time τ_{del} between the instants of valve opening and laser pulse arrival (found to be zero). These parameters remained invariable in subsequent experiments. The residence time of valves in the open state greatly exceeds the settling time for a steady-state gas flow.

3. Krypton emission spectra

Figure 2 shows the krypton emission spectra measured in the range of 8–14 nm for different krypton pressures at the capillary inlet.

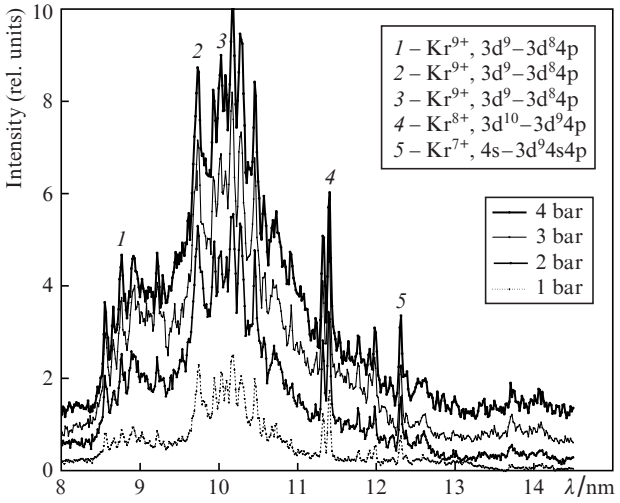

Figure 2. Emission spectra of krypton at different pressures at the capillary inlet. The spectrometer axis is oriented perpendicular to the jet axis.

The distance from the laser breakdown region to the capillary outlet is 0.5 mm. One can see a wide strong band in the range of 8–14 nm, which is due to the $3d^9-3d^84p$ fine-structure transition for Kr^{9+}, the $3d^{10}-3d^94p$ transition for Kr^{8+}, and the $4s-3d^94s4p$ transition for Kr^{7+} [36, 37]. The emission observed is due to the recombination processes occurring in

the laser plasma. An increase in the krypton pressure significantly increases the intensity of emission spectra, whereas their shape changes only slightly.

One of the key factors affecting the results of measuring the conversion efficiency of laser energy (or energy of any other type) into X-rays is the absorption of the emerging radiation by plasma and surrounding gas. To estimate this effect, we compared the shapes of the spectra recorded in two geometries: with the spectrometer axis oriented (i) perpendicular to the jet axis (providing minimum absorption) and (ii) along the jet axis (providing maximum absorption). The spectra in Fig. 3 were recorded (at a pressure of 4 bar at the nozzle inlet and at a distance of 0.5 mm from the discharge zone to the capillary edge) in two geometries: with the spectrometer optical axis oriented perpendicular and parallel to the capillary axis [curves (*1*) and (*2*), respectively]. Curve (*3*) is the spectral dependence of krypton absorption at a pressure of 1 Torr for a length of 1 cm. It can be seen that the krypton emission spectra recorded under different conditions have a similar shape. The differences are due to the larger background in the RSM-500 spectrometer and poorer resolution of the Czerny–Turner spectrometer. This fact indicates that the self-absorption is insignificant for krypton in a gas jet. This situation radically differs from that with xenon used as a gas target, where the self-absorption affects both the spectral shape and the measured signal amplitude [35].

It is of interest to compare the emission spectra of xenon and krypton. Figure 4 shows the normalised krypton and xenon emission spectra [curves (*1*) and (*2*), respectively], recorded under the following conditions. For xenon, the pressure at the capillary inlet is 2 bar and the distance from discharge region to the capillary edge is 0.5 mm; for krypton, the pressure at the nozzle inlet is 4 bar and the distance from the discharge region to the capillary edge is 0.5 mm. The intensity is shown for the same detector sensitivity; the peak in the krypton spectrum is blue-shifted, which is an advantage for lithographic applications and indicates good prospects of sources of this type.

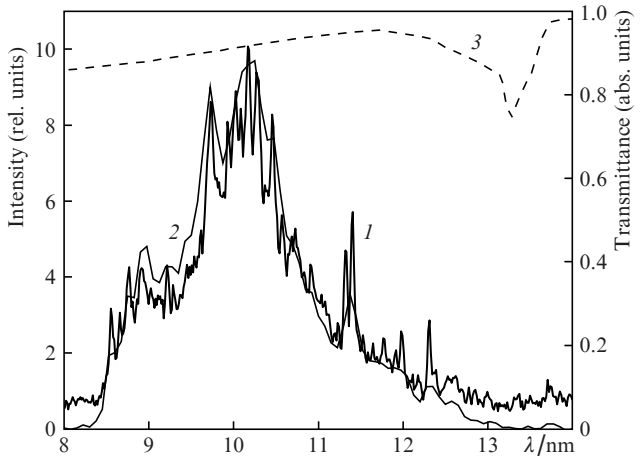

Figure 3. (*1*,*2*) Krypton emission spectra for the spectrometer optical axis oriented (*1*) perpendicular and (*2*) parallel to the capillary axis and (*3*) the spectral dependence of krypton absorption.

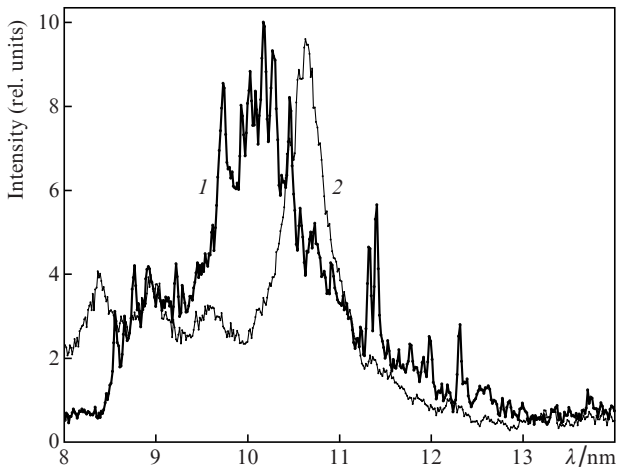

Figure 4. Emission spectra of (*1*) krypton and (*2*) xenon.

4. Measurements of the laser conversion efficiency into the krypton emission band

To determine the conversion efficiency of the laser pulse energy into short-wavelength radiation, we used a power meter (see Fig 1) allowing for measuring the total SXR energy incident on it. At the same time, the spectral dependence of radiation intensity was determined using a grating monochromator. A free-standing thin-film Mo/$ZrSi_2$ filter was also mounted at the spectrometer-monochromator input to suppress the background. In the absence of self-absorption in the plasma and gas, and with allowance for the measured spectral dependences of diffraction grating efficiency, specular reflectances, free-standing filter transmittances [18], and detector sensitivity [38], the spectra at the power meter input were reconstructed. Figure 5 shows an emission spectrum illustrating the application of this method for determining the conversion efficiency. Curve (*1*) corresponds to the reconstructed spectrum at the power meter input, and curve (*2*) is the spectrum of radiation incident on the semiconductor detector after passing through the double Mo/$ZrSi_2$ filter. Since the silicon detector sensitivity in the range of 4–14 nm barely depends on wavelength [33], the power meter signal is determined by the integral over curve (*2*), and the total X-ray energy is determined by the integral under curve (*1*).

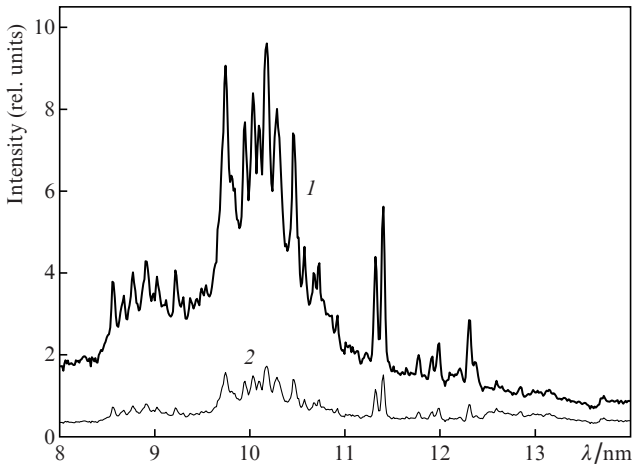

Figure 5. Reconstructed spectra, illustrating the method for determining the conversion efficiency (*1*) in the absence of filter and (*2*) after passing radiation through a double Mo/$ZrSi_2$ filter (*2*).

The conversion efficiency into half-space in the spectral range of 8–14 nm can be found from the following relations. The power W of SXR source per unit solid angle in the spectral range of 8–14 nm is given by the expression

$$W \cong \frac{KV}{\Omega ST}\frac{I}{I_{\text{tot}}}[\text{W sr}^{-1}], \quad (1)$$

where V is the detector signal (in volts), Ω is the solid angle within which the radiation is collected (7.5×10^{-4} sr), S is the detector sensitivity (0.21 A W^{-1}), T is the transmittance of double Mo/$ZrSi_2$ filter at $\lambda = 10.3$ nm (centre wavelength of the emission band), I is the intensity in the spectral range of 8–14 nm, I_{tot} is the total intensity, and K is the amplifier sensitivity (10^{-6} A V^{-1}). On the assumption of isotropic emission, the conversion efficiency of laser power P_{las} into the SXRs emitted into half-space (2π sr) is found from the relation

$$CE = 2\pi\frac{W}{P_{\text{las}}}100\ [\%], \quad (2)$$

where CE is the conversion efficiency. Thus, we obtained dependences of the laser radiation conversion efficiency in SXR on the pressure and distance from the spark to the capillary edge. The corresponding results for a pure krypton jet are presented in Fig. 6.

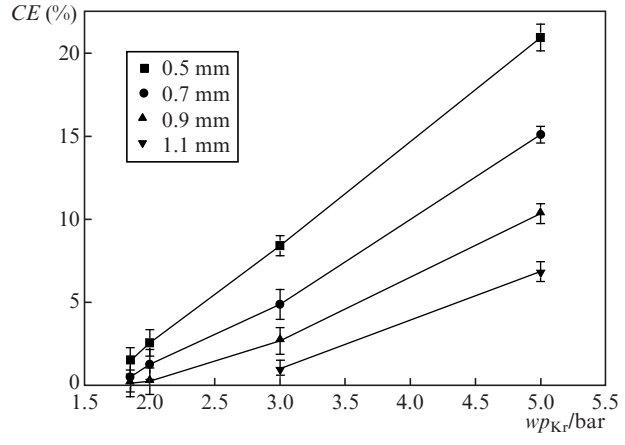

Figure 6. Dependences of the conversion efficiency CE in the (8–14)-nm band for pure krypton on the gas pressure, at different distances between the laser spark and capillary edge.

Note that an increase in the gas pressure at the capillary inlet leads to an increase in the conversion efficiency to 21% at a krypton pressure of 5 bar at the capillary inlet and a distance 0.5 mm from the laser spark to the nozzle edge. The obtained values of the conversion efficiency show that a laser-excited krypton jet may be an efficient SXR source for different applications.

5. Comparison of the characteristics of lithographic systems operating at different wavelengths

The study of the emission spectrum and conversion efficiency CE of krypton made it possible to perform a comparison with the corresponding characteristics of other SXR sources, such as the tin-ion source working at a wavelength of 13.5 nm [39] and the xenon-ion source operating at wavelengths $\lambda = 10.8$ and 11.2 nm [18]. The chosen multilayer structures for each wavelength were briefly discussed above; a more complete analysis can be found in [18]. In this paper we restricted ourselves to multilayer mirrors with maximum theoretically attainable reflectances for the chosen wavelength. The measure of the efficiency of system was taken to be the quantity PLP_{os}, found in the following way. First we determined the EF_{os} value, which is the ratio of the area under the rocking curve I_{opt} of a multimirror system to the area under the emission band I_{l}; it characterises the fraction of the emission band captured by the optical system:

$$EF_{\text{os}} = I_{\text{opt}}/I_{\text{l}}. \quad (3)$$

Then

$$PLP_{\text{os}} = R^N EF_{\text{os}}\, CE\ [\%], \quad (4)$$

where R is the maximum reflectance of a single mirror (in absolute units) and N is the number of mirrors in the system. Figure 7 presents the source spectrum [curve (*1*)] and the spectral dependence of the reflectance of five mirror systems based on the multilayer Rh/Sr structure [curve (*2*)].

Table 1 contains the calculated characteristics of a five-mirror optical system. It can be seen that the calculated characteristics of both xenon- and krypton-based lithographic systems are 3 to 4 times worse than those of a lithographer with an EUV source based on tin ions ($\lambda = 13.5$ nm).

Note that the efficiency of the Kr-based source ($\lambda = 10.3$ nm) even slightly exceeds that of the Xe source at $\lambda = 10.8$ nm. Due to the technical simplicity and purity (absence of drops and other solid-state products of tin erosion) and low cost of krypton (as compared with xenon), the krypton source is of great interest, primarily for the X-ray maskless lithography, where the throughput is not a key parameter. Obviously, concerning practical applications, the wavelength (and, correspondingly,

Table 1. Characteristics of a five-mirror optical system implemented on different multilayer mirrors.

Mirror	λ/nm	$\Delta\lambda$/nm	Target	$EF_{\text{os}}CE$ (%)	R^5	PLP_{os} (%)	References
Mo/Si	13.5	0.27	Sn	5	0,023	0.115	[35]
Ru/Be	11.2	0.208	Xe	0.42	0.292	0.122	[18]
Rh/Sr	10.8	0.247	Xe	1.65	0.220	0.363	[18]
Rh/Sr	10.8	0.247	Kr	0.89	0.220	0.023	This paper
Rh/Sr	10.3	0.209	Kr	1.31	0.234	0.040	This paper
Rh/Sr	9.85	0.17	Kr	1.01	0.211	0.024	This paper

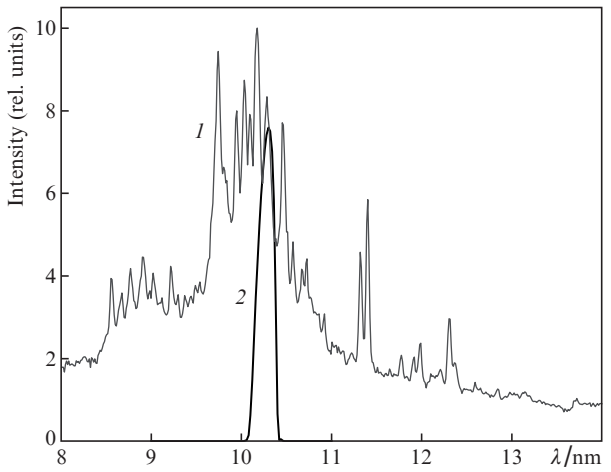

Figure 7. (*1*) Emission band of a krypton-based SXR source and (*2*) the spectral dependence of the reflectance of five-mirror system based on a multilayer Rh/Sr structure.

the radiation source) can be chosen only after obtaining experimental data on the reflectance of multilayer mirrors in a given spectral range.

6. Results and discussion

The study of the emission spectra of krypton plasma confirmed on the whole the main regularities observed by other researchers, in particular, the fact that the emission maximum corresponds to the wide (8–14 nm) band (which is due to the $3d^9-3d^84p$ fine-structure transition for Kr^{9+} ions and to the $3d^{10}-3d^94p$ and $4s-3d^94s4p$ transitions for Kr^{8+} and Kr^{7+} ions, respectively). The emission band is peaking at a wavelength of 10.3 nm.

The dependences of the laser energy conversion efficiency in the spectral range of 8–14 nm (emitted into half-space) on the krypton pressure at the pulsed-valve inlet and on the distance between the spark region and capillary edge were measured. The maximum conversion efficiency turned out to be 21%, which is indicative of a very high degree of conversion of laser radiation into EUV, approaching 50% in 4π sr. Using this measurement result and the emission spectrum, one can determine the SXR energy in the transmission band of the optical system; in particular, compare the characteristics of lithographic systems based on different radiation sources and multilayer mirrors. This comparison showed that, despite the fact that the throughput of the lithographic process with a krypton source at a wavelength of 10.3 nm is worse by a factor of about 2.8 than that for a tin-based source at $\lambda = 13.5$ nm, it somewhat exceeds the throughput of the xenon source at $\lambda = 10.8$ nm. Note that this decrease in wavelength improves the lithography resolution (limited by diffraction) by a factor of 1.3. This radiation source may be of interest for the lithographic processes where the emphasis is on the availability of equipment, low cost, and simplicity of exploitation rather than on the throughput. This primarily holds true for X-ray maskless lithography.

We should note an emission line at a wavelength of 9.85 nm, which is constantly present in the krypton emission spectrum. Therefore, the lithography operating wavelength may be shifted to the range below 10 nm. Note also that the resulting conversion efficiency did not reach saturation in terms of increasing the gas pressure at the capillary inlet. In our case the maximum pressure of 5 bar is a limit determined by the pumping system potential; therefore, one would expect a further increase in *CE* with an increase in the krypton pressure.

Finally, an unsolved problem is the determination of the limiting possibilities of Sr-based multilayer mirrors. In particular, in the early studies the reflectance of Mo/Sr mirrors under normal incidence conditions was found to be ~50% (the theoretical limit is 74%) [16]. Therefore, to determine the prospects of (10–11)-nm lithography, one must analyse the limiting possibilities of multilayer Sr-based X-ray mirrors, as well as alternative multilayer mirrors based on phosphorus compounds [40].

Acknowledgements. This work was supported by the Russian Science Foundation (Grant No. 17-12-01227) and the Russian Foundation for Basic Research (Grant Nos 18-02-00173, 18-32-00671, 19-07-00173, and 19-02-00081).

References

1. Jones S. https://seekingalpha.com/article/4151376-tsmc-intel-lead-semiconductor-processes (2018).
2. Kim S.S. et al. *Proc. SPIE*, **10143**, 1014306 (2017).
3. Migura S. et al. *Proc. SPIE*, **9661**, 96610T (2015).
4. Pirati A. et al. *Proc. SPIE*, **10143**, 101430G (2017).
5. Salashchenko N.N., Chkhalo N.I. *Herald Russ. Acad. Sci.*, **78**, 279 (2008) [*Vestn. Ross. Akad. Nauk*, **78**, 450 (2008)].
6. Wagner C., Harned N. *Nature Photon.*, **4**, 24 (2010).
7. Chkhalo N.I., Salashchenko N.N. *AIP Advances*, **3**, 082130 (2013).
8. Chkhalo N.I. et al. *Appl. Phys. Lett.*, **102**, 011602 (2013).
9. Churilov S.S. et al. *Phys. Scr.*, **80**, 045303 (2009).
10. Otsuka T. et al. *Appl. Phys. Lett.*, **97**, 111503 (2010).
11. Abramenko D.B. et al. *Proc. 17 Int. Symp. "Nanophysics & Nanoelectronics"* (Nizhny Novgorod, Russia, 2013) p. 261.
12. Stamm U. et al. *Proc. SPIE*, **5037**, 119 (2003).
13. Kieft E.R. et al. *Phys. Rev. E.*, **71**, 036402 (2005).
14. Rakowski R. et al. *Appl. Phys. B.*, **101**, 773 (2010).
15. Montcalm C. et al. *Proc. SPIE*, **3331**, 42 (1998).
16. Sae-Lao B., Montcalm C. *Opt. Lett.*, **26**, 468 (2001).
17. Chkhalo N.I. et al. *Appl. Phys. Lett.*, **112**, 221101 (2018).
18. Chkhalo N.I. et al. *AIP Advances*, **8**, 105003 (2018).
19. Fiedorowicz H. et al. *Opt. Commun.*, **163**, 103 (1999).
20. Butorin P.S. et al. *Tech. Phys.*, **63**, 1507 (2018) [*Zh. Tekh. Fiz.*, **88**, 1554 (2018)].
21. Kalmykov S.G. et al. *J. Appl. Phys.*, **126**, 103301 (2019).
22. Mizoguchi H. et al., in *Proc. 2018 China Semicond. Technol. Intern. Conf.* (CSTIC) (Shanghai, 2018) pp 1–7.
23. Choksi N. et al. *J. Vac. Sci. Technol. B*, **17**, 3047 (1999).
24. Chkhalo N.I. et al. *Proc. SPIE*, **10224**, 102241o (2016).
25. Salashchenko N.N. et al. *J. Surf. Invest.*, **12**, 944 (2018) [*Poverkhnost*, (10), 10 (2018)].
26. Chkhalo N. et al. *J. Vac. Sci. Technol. B*, **35**, 062002 (2017).
27. Fiedorowicz H. *Appl. Phys. Lett.*, **62**, 2778 (1993).
28. Nechay A.N. et al. *Poverkhnost. Rentgenovskie, Sinkhrotronnye Neitr. Issled.*, (9), 83 (2019).
29. Chkhalo N.I. et al. *J. Micro/Nanolith. MEMS MOEMS*, **11**, 021123 (2012).
30. Rakowski R. et al. *Appl. Phys. B.*, **101**, 773 (2010).
31. Fiedorowicz H. *Laser Part. Beams*, **23**, 365 (2005).
32. Garakhin S.A. et al. *Quantum Electron.*, **47**, 385 (2017) [*Kvantovaya Elektron.*, **47**, 385 (2017)].
33. Aruev P.N. et al. *Quantum Electron.*, **42**, 943 (2012) [*Kvantovaya Elektron.*, **42**, 943 (2012)].
34. Bibishkin M.S. et al. *Proc.SPIE*, **5401**, 8 (2004).

35. Belik V.P. et al. *Tech. Phys. Lett.*, **43**, 1001 (2017) [*Pis'ma Zh. Tekh. Fiz.*, **43** (22), 10 (2017)].
36. Saloman E. *J. Phys. Chem. Reference Data*, **36**, 215 (2007).
37. Reader J. et al. *JOSA B*, **2** (3), 417 (1985).
38. Kowalski M.P. et al. *Appl. Opt.*, **25**, 2440 (1986).
39. Cummings A. et al. *J. Phys. D: Appl. Phys.*, **38**, 604 (2005).
40. Medvedev V.V. et al. *Opt. Mater. Express*, **5**, 1450 (2015).